

# Seismic Assessment of Stone Arched Bridges

**J. Kiyono & A. Furukawa**

*Department of Urban Management, Kyoto University, Kyoto*

**K. Toki**

*Disaster Mitigation of Urban Cultural Heritage, Ritsumeikan University, Kyoto*



## SUMMARY:

There are many historic stone arched bridges in Japan. To prevent their damage due to earthquakes and to leave them for posterity, it is important to understand their structural integrity and failure mechanism against earthquakes. In this study, dynamic behaviors of several stone arched bridges are simulated using the 3-dimensional DEM. Firstly, by inputting a impulse wave to the models as an input ground motion, their first natural frequencies in three directions are computed, and their vibration characteristics are investigated. Secondly, seismic behaviors are computed and the failure occurrence mechanism is investigated. Effects of the material properties of the backfill and the span length on seismic behaviors and failure patterns are also investigated. Finally, effectiveness of reinforcement by inserting mortar between stones is verified.

*Keywords: historic stone arched bridge, seismic assessment, distinct element method*

## 1. INTRODUCTION

Masonry arches are one of the oldest structural elements that have been used for thousands of years as parts of bridges, tunnels, vaulted roofs, etc. There are many masonry arched structures which are designated as world heritages.

Stone arched bridges are one of the most familiar arched structures consists of stones. In Japan, many stone arched bridges were constructed before the early Meiji era when Western construction techniques were introduced. Since stones have corrosion resistance, many stone arched bridges are still standing, and some of them are valued as local historic cultural heritages.

Two stones in contact have strong resistance against compression force, but they cannot resist against any tension force. Stone arched bridges can transmit vertical loads, such as self-weight and live loads from pedestrians or vehicles, to the ground by converting the vertical load to the compression force between stones by arching effect. There have been several researches on assessing the structural integrity against the vertical loads (Jiang and Esaki, 2000; Toth et al., 2009; Betti et al., 2007), and it is well known that the stone arches have strong resistance against the vertical load. Recently, a research for preserving a historic stone arched bridge is also conducted. Structural integrity of Nishida Bridge, a stone arched bridge in Kagoshima, Japan, built about 150 years ago, was assessed in detail (Jiang and Esaki, 2000). Focusing on the weathering problem, the geometrical and mechanical parameters affected by the weathering are evaluated and its structural integrity against vertical load is confirmed by 2-dimensional distinct element method.

Seismic loads, on the contrary, act in the horizontal directions, and they are converted to both the compression and tension forces by arching effect. Most of the researches on stone arched bridges are based on the static method against self-weight or live loads in 2-dimensional analysis (Jiang and Esaki, 2000; Toth et al., 2009; Betti et al., 2007), and researches based on the dynamic analysis considering the horizontal seismic load is still scant (Rafiee et al., 2008). Since the failure behavior is 3-dimensional, the analysis in 3-dimensional is necessary, but the researches considering 3-dimensional behaviors are also still scant. One of the reasons is because the numerical tool to predict 3-dimensional dynamic behavior of masonry arches has not been established yet. Therefore, seismic resistance of the stone arched bridges and their failure mechanism during earthquakes is not fully

understand, and it is an urgent need to develop a numerical tool for predicting failure behaviors, and to investigate how the stone arched bridges get damage due to earthquakes.

With this background, this research aims to numerically assess the structural integrity of masonry stone arch bridges against seismic load using the 3-dimensional distinct element method developed by the first author. As the stone arched bridge is a discontinuous structure comprised of stones, the mechanical behavior of the stability is mainly controlled by the contact problem between stones, so we considered the distinct element method is an appropriate choice (Cundall, 1974). Based on the geometrical and material properties of Nishida Bridge that can be found in the literature (Jiang and Esaki, 2000) several models are created; a single arched ring model, an arched model with backfill made of stones, an arched model with backfill made of stones and soil, two-span arched bridges with backfill made of stones, etc. Firstly, by inputting an impulse wave to the models as an input ground motion, their first natural frequencies in three directions are computed, and their vibration characteristics are investigated. Secondly, seismic behaviors are examined and the failure occurrence mechanism is investigated. Effects of the material properties of the backfill and the span length on seismic behaviors and failure patterns are also investigated. Finally, effectiveness of reinforcement by inserting mortar between stones is verified.

## 2. ANALYSIS METHOD

### 2.1. Distinct Element Method

The DEM is a numerical analysis method that computes the position of individual elements by solving equations of motion step by step. All the elements are assumed to be rigid. Virtual springs and dashpots in the normal and tangential directions are generated when an element comes in contact with other elements, and the contact force acts through these generated virtual springs and dashpots. By solving the equation of motion for each element step by step, the behavior of all elements in combination can be traced. The forces acting on an element are the external force ( $\vec{f}$ ), and the sum of the contact forces between elements ( $\vec{F}$ ). Acceleration ( $\vec{\ddot{x}}$ ) of an element is calculated by

$$\vec{\ddot{x}} = (\vec{f} + \sum \vec{F}) / m \quad (2.1)$$

where  $m$  is the element's mass. The velocity and displacement of each element can be calculated by:

$$\vec{\dot{x}}_t = \vec{\dot{x}}_{t-\Delta t} + \vec{\ddot{x}}_{t-\Delta t} \Delta t \quad \vec{x}_t = \vec{x}_{t-\Delta t} + \vec{\dot{x}}_{t-\Delta t} \Delta t \quad (2.2)$$

where  $\Delta t$  is the time increment in the analysis.

Rotation is obtained from Euler's equations of motion. An equations for the  $\xi, \eta, \zeta$ -directions are

$$\begin{aligned} I_\xi \frac{d\omega_\xi}{dt} - (I_\eta - I_\zeta) \omega_\eta \omega_\zeta &= (\sum_i r_i \times F_i)_\xi & I_\eta \frac{d\omega_\eta}{dt} - (I_\zeta - I_\xi) \omega_\zeta \omega_\xi &= (\sum_i r_i \times F_i)_\eta \\ I_\zeta \frac{d\omega_\zeta}{dt} - (I_\xi - I_\eta) \omega_\xi \omega_\eta &= (\sum_i r_i \times F_i)_\zeta \end{aligned} \quad (2.3)$$

in which  $\xi, \eta$ , and  $\zeta$  are the inertia axes of the coordinates, and  $I_i$  and  $\omega_i$  ( $i = \xi, \eta, \zeta$ ) respectively are the moments of inertia and rotational velocities around the center of gravity in the inertial frame of reference.  $r_i$  ( $i = \xi, \eta, \zeta$ ) is the distance between the center of the gravity and the point where the contact force,  $F_i$ , is applied.

### 2.2 Simplified micro-modeling of masonry structure

To predict the dynamic behavior of a masonry structure using the DEM, micro-modeling of individual components, i.e. block and mortar, is necessary. In this paper, these components are modeled in a simple manner as shown in **Fig. 1(a)** according to the past research (Lourenco, 1994). The blocks are called units and the mortar conjunction between units is called a joint. The size of one unit is the sum of brick size and mortar thickness. The unit is modeled as a distinct element. The joint has zero thickness and interacts with the surfaces of adjacent units. Even for the case when there is no mortar between blocks, the same modeling can be used assuming that the joint has no tension and bonding strengths.

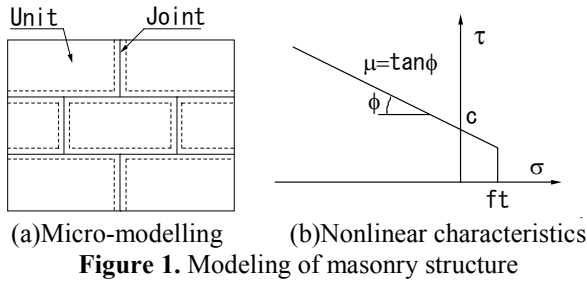


Figure 1. Modeling of masonry structure

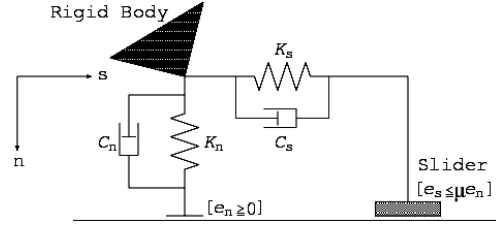


Figure 2. Contact between elements.

### 2.3 Contact Force

When elements (units) come into contact or connected by joint, the spring and dashpot are generated in the calculation. The contact model shown in Fig. 2. is the case in which a corner of element is in contact with the other element's face or edge. Judgment of contact is made by considering the collocation between the two elements concerned. Increments in the spring and damping forces in the normal and tangential directions ( $\Delta e_n$ ,  $\Delta e_s$ ,  $\Delta d_n$ ,  $\Delta d_s$ ) for the interval  $\Delta t$  are expressed by the increments of relative displacement in those directions,  $\Delta n$  and  $\Delta s$ ;

$$\Delta e_n = K_n \Delta n \quad \Delta e_s = K_s \Delta s \quad \Delta d_n = C_n \Delta n / \Delta t \quad \Delta d_s = C_s \Delta s / \Delta t \quad (2.4)$$

in which  $K_n$  and  $K_s$ , and  $C_n$  and  $C_s$ , respectively are the spring constants and damping coefficients in the normal and tangential directions. The spring and damping forces in each direction ( $[e_n]_t$ ,  $[e_s]_t$ ,  $[d_n]_t$ ,  $[d_s]_t$ ) at the arbitrary time  $t$  are obtained from the preceding equations;

$$[e_n]_t = [e_n]_{t-\Delta t} + \Delta e_n \quad [e_s]_t = [e_s]_{t-\Delta t} + \Delta e_s \quad [d_n]_t = \Delta d_n \quad [d_s]_t = \Delta d_s \quad (2.5)$$

When the spring force exceeds the tension, shear or compression strength, the contact force is governed by the nonlinear characteristics shown in 2.4. The total contact forces in both directions are

$$[F_n]_t = [e_n]_t + [d_n]_t \quad [F_s]_t = [e_s]_t + [d_s]_t \quad (2.6)$$

Force,  $F$  in Eq. (1) is obtained by combining the above forces in the target direction.

### 2.4 Nonlinear Characteristics of Contact Force

The contact force is generated at contact points when two units with or without mortar between them are in contact with each other. The mechanical characteristics of contact force are modeled by introducing nonlinear characteristics to the contact force. The three failure modes, namely tension mode and shear mode are defined according to the past research (Lourenco, 1994). Here we regard the normal spring force,  $[e_n]_t$ , per area as normal stress  $\sigma$ , and the tangential spring force,  $[e_s]_t$ , per area as shear stress  $\tau$ . The failure criterion as a relationship between the normal stress  $\sigma$  and the shear stress  $\tau$  is shown in Fig. 1.(b).

#### 2.4.1 Tension mode

In the tension mode, the necessary parameter is the tensile strength  $f_t$ . The yield function is as follows.

$$f_1(\sigma) = \sigma - f_t \quad (2.7)$$

When it reaches this limit, damping force is set 0.

#### 2.4.2 Shear mode

For the shear mode, the Coulomb friction envelope is used. The required parameters are the bond strength  $c$ , and the friction angle,  $\phi$ . The yield function has the following form.

$$f_2(\sigma) = |\tau| + \sigma \tan \phi - c \quad (2.8)$$

When the spring force exceeds this friction limit, the tangential force is governed by the dynamic friction and damping force is set 0. If stones are not bonded with each other by mortar,  $f_t$  and  $c$  are set to 0.

### 2.5 Spring constants and damping coefficients

It is assumed that two elements,  $A$  and  $B$ , are in contact, and that a contact area is  $S$ . Let  $G_A$  and  $G_B$  be the centers of gravity of elements  $A$  and  $B$  respectively. Let  $\ell_A$  be the distance from  $G_A$  to the contact

area. Let  $\ell_B$  be the distance from  $G_B$  to the contact area. Let  $E_A$  and  $E_B$  be Young's modulus and  $\nu_A$  and  $\nu_B$  be Poisson's ratios of elements  $A$  and  $B$ .

The spring constants in the normal and tangential directions,  $K_n$  and  $K_s$ , are

$$K_n = \frac{S}{\frac{\ell_A}{E_A/(1-\nu_A^2)} + \frac{\ell_B}{E_B/(1-\nu_B^2)}} \quad K_s = \frac{S}{\frac{\ell_A}{E_A/2(1+\nu_A)} + \frac{\ell_B}{E_B/2(1+\nu_B)}} \quad (2.9)$$

Damping coefficients in the normal and tangential directions are assumed as

$$C_n = 2h_n\sqrt{m_{ave}K_n} \quad C_s = 2h_s\sqrt{m_{ave}K_s} \quad (2.10)$$

where,  $h_n$ ,  $h_s$  are damping constants of the dashpots.  $m_{ave}$  is an equivalent mass of the contact, and obtained as follows

$$m_{ave} = (\rho_A\ell_A + \rho_B\ell_B)S \quad (2.11)$$

where  $\rho_A$  and  $\rho_B$  are densities of elements  $A$  and  $B$ .

### 3. ANALYSIS OUTLINE

#### 3.1 Input Ground Motion

Acceleration records obtained at the Kobe Marine Observatory during the 1995 Hyogo-ken Nanbu earthquake is used (Fig.3.). EW, NS and US components are input in  $x$ ,  $y$  and  $z$  directions, respectively.

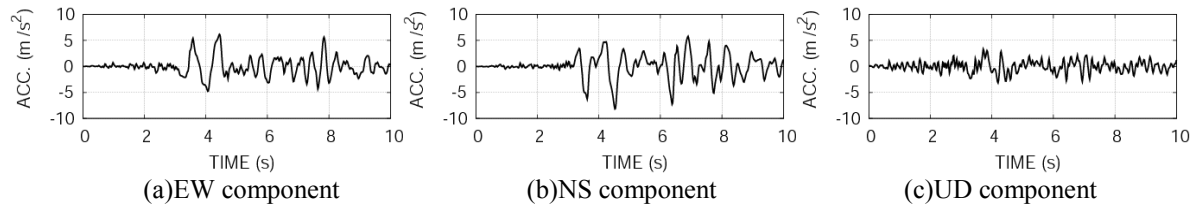


Figure 3. Input ground motion

#### 3.2 Analytical models

Nishida Bridge is a four-span structure. The geometry of the second span from the upper stream view was illustrated by Jiang and Esaki (2000) based on the in situ survey. Six analytical models are created based on the second span of Nishida Bridge as shown in Fig. 4. The actual width of Nishida bridge with four spans are 6.2m, but the analyzed models with single or two spans are set to be 3.2m. The models are assumed to be constructed on the fixed ground. The directions of input ground motion are shown in Fig. 4. (a). The details of each model are as follows.

##### 3.2.1 Model A

Model A has only an arched ring. The model has a span length of 11.36 m, rise height of 4.76 m, and thickness of 0.64 m in accordance with the literature (Jiang and Esaki, 2000). The width of the bridge is assumed 3.2m, and dimensions of stones are assumed about 0.64m × 0.64m × 0.64m. The stones on the bottom are fixed. The stones are not connected with each other by mortar, and only friction force acts between stones in contact. The total number of elements is 165.

##### 3.2.2 Model B

Model B has a wall made of stones on an arched ring of model A. The height is 5.8 m in accordance with the literature (Jiang and Esaki, 2000). The length of the model is assumed to be 24m. The dimensions of stones are assumed about 0.64m × 0.64m × 0.64m. The total number of elements is 1586.

### 3.2.3 Model C

Model C has fixed side walls in addition to Model B. The width of the side walls are 1.0m. The material of the side wall is the same as those of the stones. The total number of elements is 1588.

### 3.2.4 Model D

In Model D, two walls in the front and the rear composed of stones, and soil is filled inside. Soils are simply modeled with the cubic elements with the same size of the stones. The total number of elements is 1448.

### 3.2.5 Model E

Model E has fixed side walls in addition to Model D. The total number of elements is 1450.

### 3.2.6 Model F

Model F is a two-span model with the fixed elements in the both sides. The length of the bridge is 36m. The total number of elements is 2043.

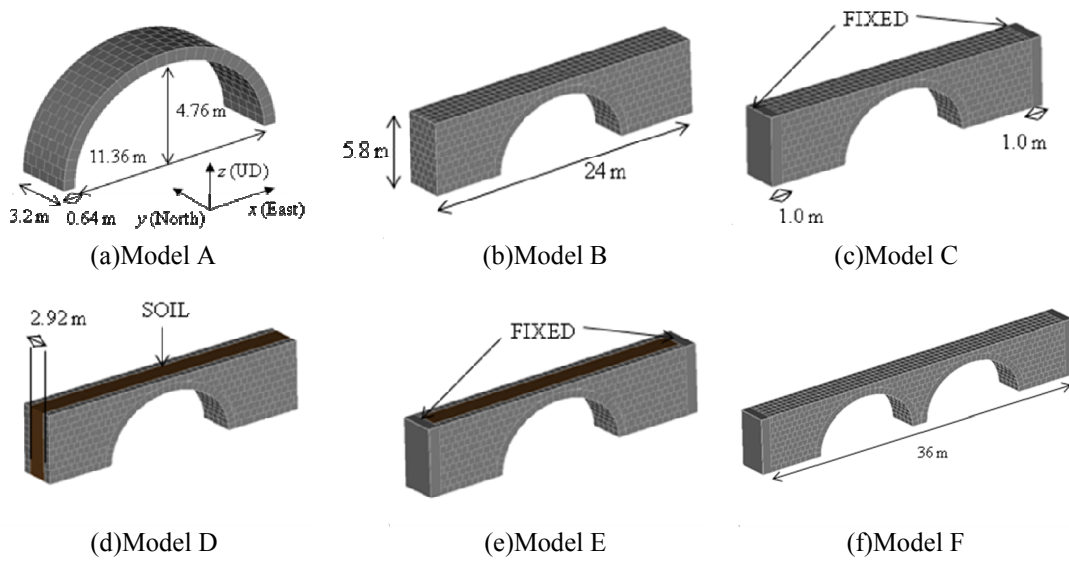


Figure 4. Analytical models.

## 3.3 Material properties

The material properties of stones are defined based on the field survey results of Nishida Bridge (Jiang and Esaki, 2000). Density of stones is  $1.88 \times 10^3 \text{ kg/m}^3$ , Young's modulus is  $1.4039 \times 10^{10} \text{ N/m}^2$ , Poisson's ratio is 0.28. As for the material properties of the ground and the soil of models D and E, density is assumed to be  $1.8 \times 10^3 \text{ kg/m}^3$ , Young's modulus is  $1.9 \times 10^8 \text{ N/m}^2$ , Poisson's ratio is 0.3. Young's modulus is defined on the assumption that the shear velocity of the soil is 200m/s. For damping, critical damping ( $h_n = h_s = 1.0$ ) is assumed. These values are used to obtain spring constants and damping coefficients in the analysis.

## 3.4 Failure criterion

Friction angle between stones is assumed to be 33.23 degree according to the literature (Jiang and Esaki, 2000), and that between soils and that between stone and soil are both assumed to be 30 degree. For all stone-stone, soil-soil, and stone-soil contacts, tensile and bond strength are assumed to be 0.0.

## 3.5. Time interval

Cundall (1974) recommends the following time interval. From this,  $\Delta t = 0.00004 \text{ (sec)}$  is adopted.

$$\Delta t < 2\sqrt{m / K_n} \quad (3.1)$$

## 4. RESULTS

### 4.1 Natural frequencies

First, natural frequencies are computed by inputting impulse waves in single direction and conducting Fourier transformation of the responses in its direction. In obtaining the responses, tensile and shear failures between stones originally in contact were neglected to obtain the linear responses.

**Table 1.** shows the first natural frequency in each direction. In model A, the first natural frequencies in  $x$  and  $z$  directions are the same and lower than that in  $y$  direction. This means that the first mode is mainly by the inner-plane ( $x$ - $z$  plane) deformation, and that the inner-plane deformation is more dominant than the out-of-plane ( $y$ - $z$  plane) deformation. In model B, on the contrary, the first natural frequencies in  $y$  and  $z$  directions are the same and lower than that in  $x$  direction. This means that the first mode is mainly by the out-of-plane deformation, and that the out-of-plane ( $y$ - $z$  plane) deformation is more dominant than the inner-plane ( $x$ - $z$  plane) deformation. This fact that the arched ring is less deformable in the inner-plane compared to model A is because of the stiff backfill made by stones. In model C, the first natural frequencies in three directions are almost the same and higher than those of models A and B due to the fixed elements in the both sides. In model D, due to the soft soil inside, the natural frequency in three directions are lower than those of model B. In model E, the natural frequencies in three directions are almost the same in the same manner as model C, but are lower than those of model C due to the soft soil. In model F, the natural frequencies are almost the same in three directions and smaller than those of model C due to its longer span length.

**Table 1.** 1<sup>st</sup> natural frequency in each direction

	Model A	Model B	Model C	Model D	Model E	Model F
$x$	17.6 Hz	23.9 Hz	30.2 Hz	16.8 Hz	17.1 Hz	12.4 Hz
$y$	24.7 Hz	17.1 Hz	30.2 Hz	9.5 Hz	17.1 Hz	12.4 Hz
$z$	17.6 Hz	17.1 Hz	30.2 Hz	9.5 Hz	17.1 Hz	12.4 Hz

### 4.2 Seismic behavior, model A

Seismic behavior of model A is shown in **Fig. 5**. Before 4.0 sec while the input acceleration is small, the model stand still against its self weight. At 4.0 sec, the first horizontal crack can be seen. At 4.2 sec, three cracks are found, and the arch ring are separated into 5 parts like the character of “M” at 4.4 sec, and collapsed. Inner-plane deformation is dominant. It is found that the structure is easily deformed in the inner-plane, and once the failure occurs, the structure starts to fall down due to its instable shape.

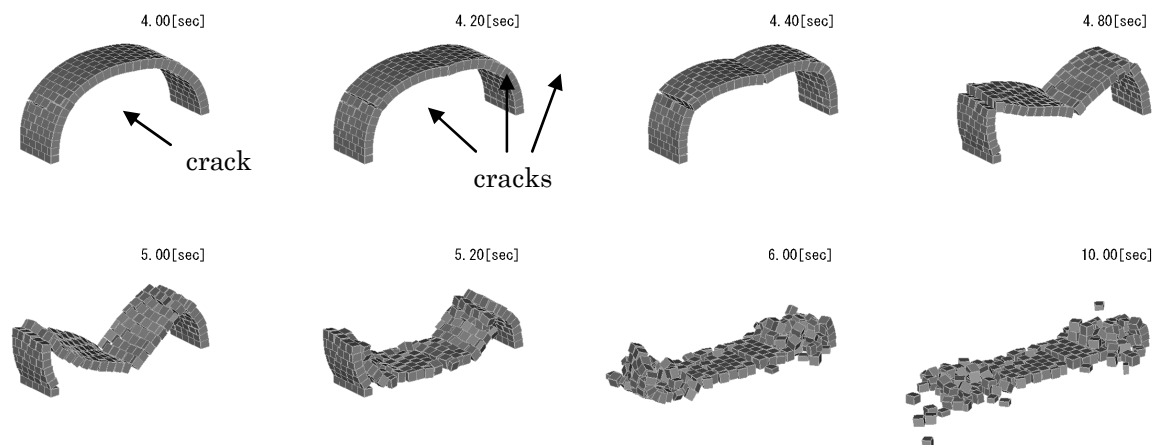


**Figure 5.** Seismic behavior, model A

### 4.3 Seismic behavior, model B

Seismic behavior of model B is shown in **Fig. 6**. At 4.0 sec, no cracks can be seen in the arched ring. Because model B has stiff backfill, the deformation of arched ring is less likely to occur. The main

deformation is the out-of-plane deformation of the walls in the both sides. At 4.4 sec, the out-of-deformation of can be seen. The walls on the left and right sides move in the opposite directions, and this causes the torsional behavior. Due to this torsional behavior, cracks are generated as can be seen in the picture of 4.8 sec. At 5.2 sec, stone elements in the left sides started to fall down due to its larger out-of-plane deformation, but no elements fell from the arched ring. It is found that the cracks in the arched ring are generated due to wall's out-of-plane deformation with the torsional behavior. This indicates that to assess the seismic strength of the arched structures, three-dimensional analysis is necessary.

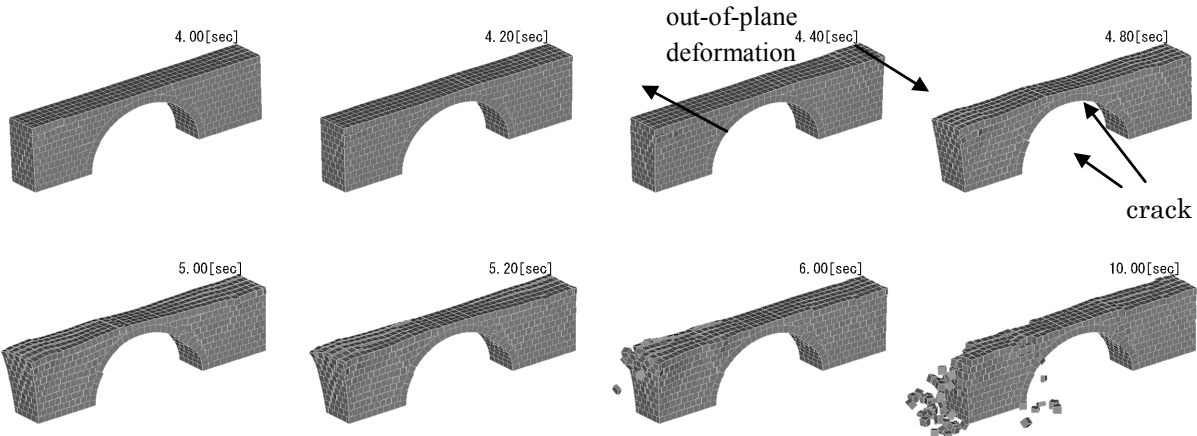


Figure 6. Seismic behavior, model B

4.4 Seismic behavior, model C

Since model C has fixed walls in the both sides, the out-of-plane deformation is very small and no clear cracks can be seen. It survived the earthquake as shown in Fig. 7.

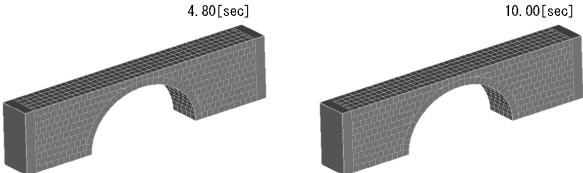


Figure 7. Seismic behavior, model C

4.5 Seismic behavior, model D

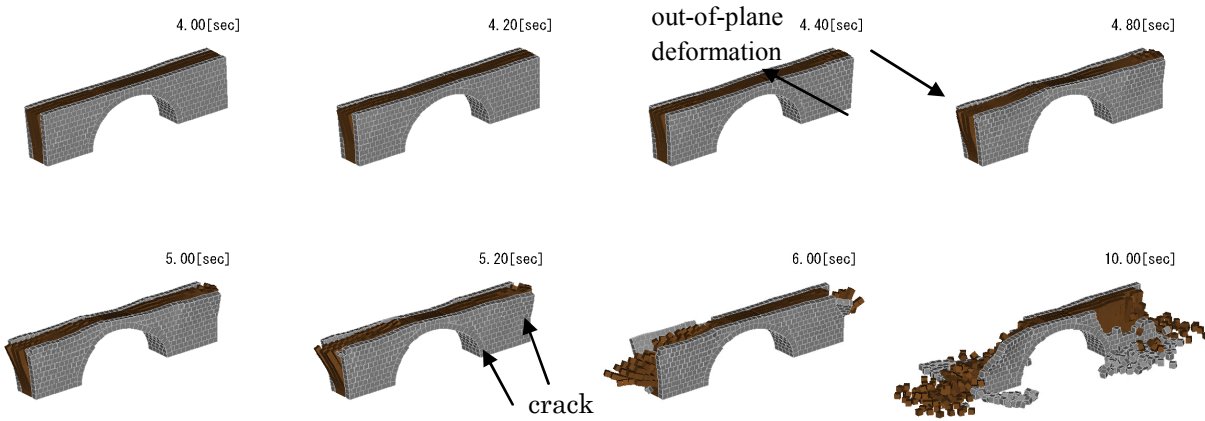
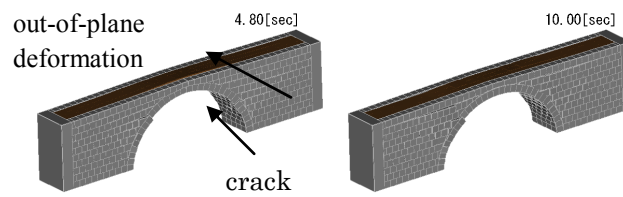


Figure 8. Seismic behavior, model D

Seismic behavior of model D is shown in **Fig. 8**. Since the wall has soil elements softer than the stone elements, the out-of-plane deformation is larger than that for model B, which can be seen by comparing the pictures of 4.8 sec in **Figs. 6** and **8**. Moreover, the stone elements and the soil elements show individual out-of-plane behavior as can be seen after 5.2 sec. The failure occurrence mechanism of model D is the same as that of model B. The wall's out-of-plane deformation with torsional behavior generated the cracks. No elements fell from the arched ring and only elements from the backfill fell down.

#### 4.6 Seismic behavior, case E

Seismic behavior of model E is shown in **Fig. 9**. Though the model has the fixed elements in the both sides, the out-of-plane deformation is larger than that of model C due to the soft soil in the backfill. Therefore, the cracks are generated as can be seen at the picture of 4.8 sec.



**Figure 9.** Seismic behavior, model E

#### 4.7 Seismic behavior, case F

Seismic behavior of model F is shown in **Fig. 10**.

Model F has the fixed elements in the both sides as similar to model C, but has longer bridge length. The out-of-plane deformation in the middle span is larger than that of model C, so the cracks are generated in this part at 4.8 sec. The cracks proceed after 7.0 sec, and several stone elements between two arched rings fell down. From these findings, it can be expected that multi-span bridges have larger out-of-plane deformation, causing more cracks in the parts between arched rings.

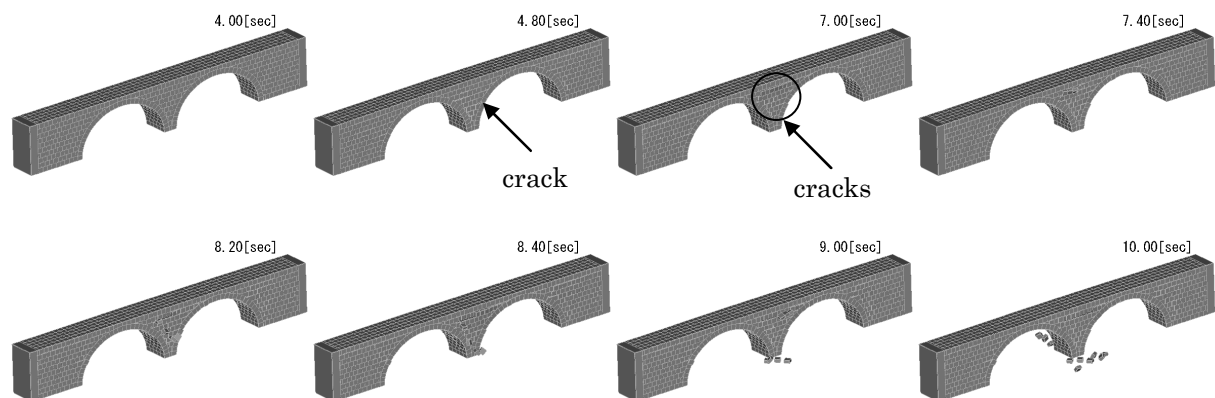


**Figure 10.** Seismic behavior, model F

#### 4.8 Vertical displacement history of top of the arched ring

Vertical displacement histories of the gravity center of the element which is on the top of the arched ring are compared in **Fig. 11**.

From **Fig. 11.(a)**, it is found that the element from model A fell down, and it started falling at about 3.5 sec when the acceleration history of the input ground motion takes large values.

As for models C, E and F with fixed elements in the both sides (**Fig. 11.(c)(e)(f)**), the vertical displacement histories have similar shapes. They have two peaks at about 3.8 sec and 4.8 sec. These two peaks come from the peaks of the input ground motions in NS ( $y$ ) direction (**Fig. 3. (b)**).

As for models B and D with no fixed elements in the sides (**Fig. 11.(b)(d)**), the vertical displacement histories have also similar shapes. They have three peaks at about 3.8, 4.3 and 4.8 sec. The peaks at 4.3 sec come from the peak ground acceleration in EW ( $x$ ) direction (**Fig. 3.(a)**). Since models B and D have no constraints in  $x$  direction and can deform in its direction, the effect of the input ground motion in EW( $x$ ) direction can be seen.

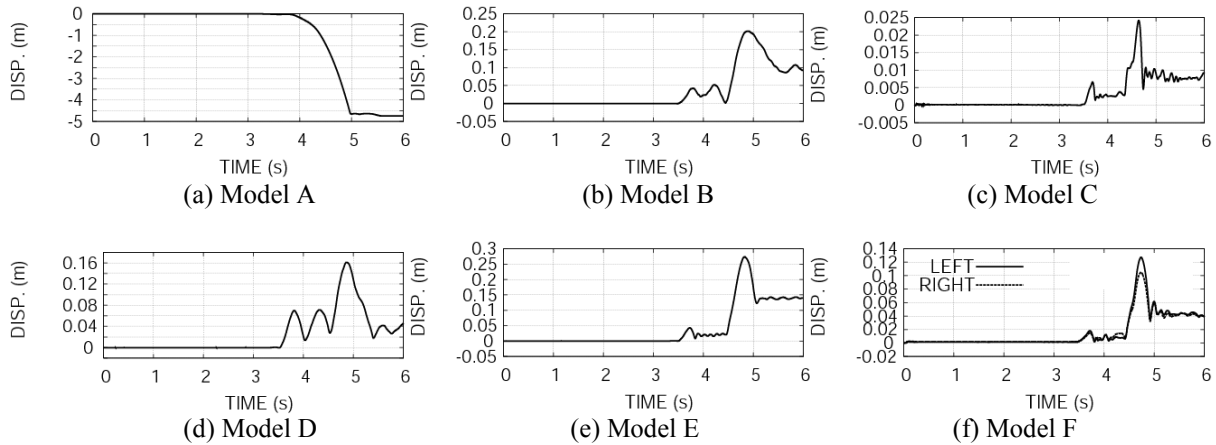


**Figure 11.** Displacement histories of elements on top of the arch ring in  $z$  direction

#### 4.9 Effect of reinforcement by inserting mortar

Next, the effect of reinforcement by mortar is investigated. All models are reinforced by inserting mortar between stones. The tension and bonding strengths between stones originally in contact are set to be  $f_t = c = 2.0 \times 10^6 \text{ N/m}^2$ . No reinforcement is made to soils in the backfill.

**Fig. 12.** indicates the reinforced models after the earthquake excitation. Reinforcement to stone walls of model D failed in resisting earthquake excitation because unreinforced soil elements moved and pushed the stone walls outward. Apart from model D, no elements fell down and the effect of the reinforcement is confirmed.

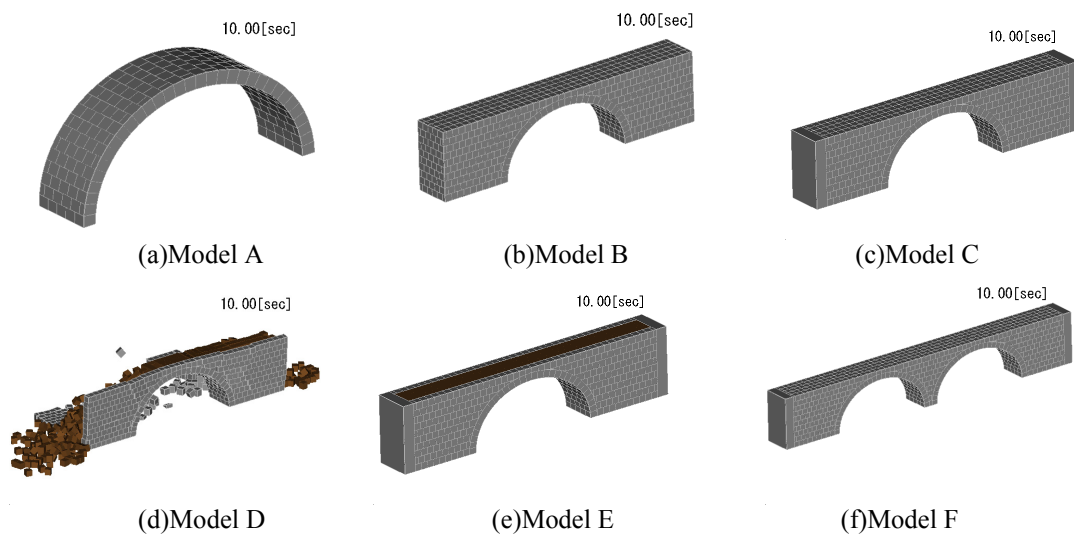


**Figure 12.** Models with mortar reinforcement

## 5. CONCLUSION

Seismic behaviors of the stone arched bridges are analyzed by the 3-dimensional DEM. The structural models are created based on the existing stone arched bridge in Kagoshima, Japan, whose geometry and material properties can be found in the literature. Several models are created, a single arched ring model, an arched model with backfill made of stones, an arched model with backfill made of stones and soil, two-span arched bridges with backfill made of stones, etc. The earthquake ground motions observed during the 1995 Hyogo-ken Nanbu earthquake are used.

Firstly, by inputting impulse wave, the first natural frequencies in three directions are computed, and their vibration characteristics are investigated. It is found that the dominant mode of the single arched ring model is an inner-plane deformation, and that the dominant mode of arched bridges with the backfill is the out-of-plane deformation. Secondly, seismic behaviors are computed and the failure mechanism is investigated. It is found that the single arched ring model is very vulnerable and collapsed by the earthquake. For other models with the backfill, the arched ring part did not collapse even though cracks occurred. The cracks occurred mainly by the out-of-plane deformation of the bridges with torsional behavior. The elements from the backfill fell down for the models without fixed elements in the sides and for the models with two-span due to their deformability in the out-of-plane direction.

All models except the single arched ring model avoided collapsing, and it is found that the analyzed stone arched bridges with backfill have the seismic resistance. However, as the number of spans increases or if the boundary condition is free in the side, or if soils are packed inside the bridges, there is a possibility that some stones fall down because the out-of-plane deformation increases. Therefore, to assess the seismic performance, appropriate modeling of the boundary conditions in the sides and the material properties in the backfill is found to be important. Seismic behaviors of reinforced models by inserting mortar between stones are also computed and the effectiveness is confirmed.

## REFERENCES

- Betti, M., Drosopoulos, G.A., Stavroulakis, G.E. (2007). On the collapse analysis of single span masonry/stone arch bridges with fill interaction. *5<sup>th</sup> International Conference on Arch Bridges*, 617-624.
- Cundall, P.A. (1974). Rational Design of Tunnel Supports: A Computer Model for Rock Mass Behavior Using Interactive Graphics for the Input and Output of Geometrical Data. *Technical Report MRD-2-74*, Missouri River Division, U.S. Army Corps of Engineers.
- Jiang, K., Esaki, T. (2000). Quantitative evaluation of stability changes in historical stone bridges in Kagoshima, Japan, by weathering. *Engineering Geology*, **63**, 83-91.
- Lourenco, P.B. (1994). Analysis of masonry structures with interface elements, theory and applications. *TU-DELFT report no.03-21-22-0-01*, *TNO-BOUW report no.94-NW-R0762*, Delft University of Technology, Faculty of Civil Engineering.
- Rafiee, A., Vinches, M., Bohatier, C. (2008). Application of the NSCD method to analyze the dynamic behaviour of stone arched structures. *International Journal of solids and structures*, **45**, 6269-6283.
- Toth, A.R., Orban, Z., Bagi, K. 2009. Discrete element analysis of a stone masonry arch. *Mechanics Research Communications*, **36**, 469-480.